



# High Catalytic Activity of $\text{Fe}_{3-x}\text{Cu}_x\text{O}_4/\text{Graphene Oxide}$ ( $0 \leq x \leq 0.1$ ) Nanocomposites as Heterogeneous Fenton Catalysts for p-Nitrophenol Degradation

Mingwang Liu · Zhenzhen Jia · Peng Li ·  
Yunfang Liu · Mengjia Zhao · Yizi Yang ·  
Qigu Huang · Changyuan Yu

Received: 10 August 2018 / Accepted: 11 February 2019 / Published online: 21 February 2019  
© Springer Nature Switzerland AG 2019

**Abstract** In order to improve the catalytic properties of  $\text{Fe}_3\text{O}_4$  nanoparticles in wastewater treatment, the Cu-doped  $\text{Fe}_3\text{O}_4/\text{graphene oxide}$  ( $\text{Fe}_{3-x}\text{Cu}_x\text{O}_4/\text{GO}$ ) nanocomposites were prepared by a modified coprecipitation method and used as heterogeneous catalyst for p-Nitrophenol (p-NP) degradation. The effect of the GO and Cu contents in the nanocomposites was investigated. Compared with the unsupported  $\text{Fe}_3\text{O}_4$  nanoparticles, the  $\text{Fe}_3\text{O}_4/\text{GO}$  nanocomposites have obviously improved catalytic performance, especially for the nanocomposite with 6.25 wt.% of the GO content. Furthermore, the catalytic efficiency is greatly improved by doping Cu in the nanocomposite. The  $\text{Fe}_{3-x}\text{Cu}_x\text{O}_4/\text{GO}$  nanocomposite achieves the best catalytic property in our catalyst system when the  $x$  value is about 0.075. Under the optimal reaction condition (0.8 g  $\text{L}^{-1}$  of catalyst dosage, 15 mmol  $\text{L}^{-1}$  of initial  $\text{H}_2\text{O}_2$  concentration, 3.0 of pH value, and 30 °C of temperature), the p-NP conversion and chemical oxygen demand removal efficiencies in 120 min for the  $\text{Fe}_{2.925}\text{Cu}_{0.075}\text{O}_4/\text{GO}$  nanocomposite are about 98.4% and 74.7%,

respectively. And the p-NP conversion efficiency is still as high as 96.2% after four recycles under the optimum condition. The results clearly show that the  $\text{Fe}_{2.925}\text{Cu}_{0.075}\text{O}_4/\text{GO}$  nanocomposite has outstanding catalytic properties for the p-NP degradation.

**Keywords** Magnetite nanocomposite · Graphene oxide · Cu doping · Heterogeneous Fenton catalyst · Wastewater treatment

## 1 Introduction

With the rapid development of economy, the environmental pollution has become more and more serious, especially for the organic pollution. Phenolic compounds have been widely used in dyes, explosives, preservatives, pesticides, plasticizers, pharmaceuticals, and leather preservatives as raw materials or intermediates, such as p-Nitrophenol (p-NP) (Wan et al. 2016). But the p-NP is a very high-stable, water-soluble,

**Electronic supplementary material** The online version of this article (<https://doi.org/10.1007/s11270-019-4121-1>) contains supplementary material, which is available to authorized users.

M. Liu · Z. Jia · P. Li · Y. Liu · M. Zhao · Y. Yang ·  
Q. Huang  
School of Material Science and Technology, Beijing University of  
Chemical Technology, Beijing 100029, China

P. Li · Y. Liu (✉) · Q. Huang  
Key Laboratory of carbon fiber and functional polymers Ministry  
of Education, Beijing University of Chemical Technology,

Beijing 100029, China  
e-mail: liuyunfang@mail.buct.edu.cn

C. Yu  
School of Life Science and Technology, Beijing University of  
Chemical Technology, Beijing 100029, China

strongly toxic, and poorly biodegradable molecular (Wang et al. 2017a, b; Zhao et al. 2010). According to the index of the United States Environmental Protection Agency (USEPA), the p-NP concentration in water environment must be lower than  $10 \text{ ng L}^{-1}$  in order to ensure our safety (Chen et al. 2017). Therefore, it is of great significance to find some efficient methods to degrade p-NP. So far, there are many technologies to treat the p-NP containing wastewater, such as Fenton degradation (Wan et al. 2016), photocatalytic degradation, adsorption, membrane filtration, and biological treatment (Yu et al. 2016).

In recent years, Fenton process has been widely used to treat the phenolic wastewater because of highly active hydroxyl radical ( $\cdot\text{OH}$ ) (Tian et al. 2017). Due to the strong oxidation ability of hydroxyl radical ( $E_0 = 2.8 \text{ V}$ ), most organic molecules could be mineralized into inorganic substances ( $\text{CO}_2$ ,  $\text{H}_2\text{O}$ , etc.) or transformed into biodegradable organic molecules (Wang et al. 2017a, b; Gonzalez-Olmos et al. 2012). Fenton process can be divided into homogeneous and heterogeneous Fenton according to catalyst state. The heterogeneous process uses the solid catalyst and has many merits, such as relatively smaller amount of iron sludge (Pugazhenthiran et al. 2011) and relatively higher  $\text{H}_2\text{O}_2$  utilization efficiency. Natural minerals have been widely applied as heterogeneous catalysts due to their large reserves and low price, such as goethite ( $\alpha\text{-FeOOH}$ ) (Kwan and Voelker 2003), hematite ( $\alpha\text{-Fe}_2\text{O}_3$ ) (Huang et al. 2001), and magnetite ( $\text{Fe}_3\text{O}_4$ ) (Matta et al. 2007) etc. But the natural magnetite generally has low catalytic ability. So, a great deal of interest has been attracted to the artificial  $\text{Fe}_3\text{O}_4$ -based catalysts due to their high catalytic activity, low cost, easily separation, and recovery (Pereira et al. 2012; Zhu et al. 2017; Zhang et al. 2009). However,  $\text{Fe}_3\text{O}_4$  nanoparticles (NPs) easily aggregate into large particles that will inevitably damage the catalytic activity. So, immobilizing  $\text{Fe}_3\text{O}_4$  on support is an effective way to solve this problem (Zubir et al. 2014).

Carbon materials (carbon nanotube (Xu et al. 2016), graphene (Zhang et al. 2009; Guo et al. 2013), and activated carbon (Kakavandi et al. 2016)) have been used as  $\text{Fe}_3\text{O}_4$  supports. Graphene oxide (GO) is particularly considered as one of the most promising materials for nanoparticle support due to its outstanding properties: (1) GO has a special two-dimensional lamellar structure with high surface area and catalytic activity (Yu et al. 2016); (2) GO has many oxygen-containing

functional groups (epoxides, ketones, and carboxyl radicals (Wu et al. 2014)) that could provide the nucleation sites for metal ions (Zubir et al. 2014); (3) furthermore, GO has a higher electron transport capacity than the metal oxides and other materials (Ullah et al. 2014). As results, the aggregation phenomenon of the nanoparticles decreases and the catalytic activity of the composites will become high due to the synergistic effect between  $\text{Fe}_3\text{O}_4$  NPs and GO (Zubir et al. 2014). Up to now, some  $\text{Fe}_3\text{O}_4/\text{GO}$  nanocomposites have been gotten as catalyst for phenol oxidation (Yu et al. 2016) and nitroarene degradation (He et al. 2013), which show good catalytic abilities.

Many studies have shown that the co-existence of  $M^{n+}/M^{(n+1)+}$  redox pairs in the octahedral sites of the spinel-structure metal oxides play a very important role in the formation of OH (Barros et al. 2016). Magnetite has a typical spinel structure (Menini et al. 2008) and could have more actively catalytic sites after isostructural substitution by other transition metals (Moura et al. 2005). As results, many  $\text{Fe}_{3-x}\text{M}_x\text{O}_4$  materials have been prepared by introducing different metal elements (Co, Cr, Ti, Mn, and so on) and used for the decolorization of methylene blue (Nejad and Jonsson 2004; Magalhães et al. 2007; Yang et al. 2009; Costa et al. 2006). Although having the “couple” ( $\text{Cu}^{2+}/\text{Cu}^+$ ), copper used alone has a very low catalytic activity as Fenton catalyst. But the  $\text{Cu}^{2+}$  ions could obviously enhance the catalytic activity of  $\text{Fe}^{2+}$  or  $\text{Fe}^{3+}$  after doping into the catalyst system (Barros et al. 2016). Therefore, it is possible to effectively improve the activity of the  $\text{Fe}_3\text{O}_4$ -based catalyst by doping Cu with an appropriate content. Up to now, there was no literature about the preparation of  $\text{Fe}_{3-x}\text{Cu}_x\text{O}_4/\text{GO}$  nanocomposite as heterogeneous Fenton catalyst for organic pollutant degradation. In this work, we prepared the  $\text{Fe}_{3-x}\text{Cu}_x\text{O}_4/\text{GO}$  nanocomposites for p-NP degradation and investigated the effect of the GO and Cu contents in the nanocomposites on the catalytic performances. And the possible catalytic mechanism was also discussed.

## 2 Experimental Procedure

### 2.1 Reagents and Materials

Sulfuric acid ( $\text{H}_2\text{SO}_4$ , 98%), potassium permanganate ( $\text{KMnO}_4$ ), ferric chloride, ferrous chloride, copper chloride, p-NP, and hydrogen peroxide ( $\text{H}_2\text{O}_2$ , 30%, w/w)

were all purchased from Tianjin Fuchen Chemical Reagents Factory (China). All of the above chemicals and reagents were of analytical grade and used without further purification. Expanded graphite (EG) was bought from Qingdao Yanhai Carbon Materials Co., Ltd.

## 2.2 Preparation of GO

The GO was prepared by a modified Hummer's method (Sun and Fugetsu 2013). First, 15 g of  $\text{KMnO}_4$  and 5 g of EG were mixed in a 500-mL round-bottom flask and kept in an ice-water bath. Then, 100 mL of concentrated sulfuric acid (98%) was dropwise added into the mixture and stirred for 0.5 h. After that, the mixture was agitated at room temperature for 1 h to form a foam-like intermediate spontaneously. Then, deionized water (400 mL) was slowly added and stirred vigorously for 1 h. Following that, the flask was stirred at 90 °C for 1 h. After reaction, the mixture was cooled to room temperature, and an appropriate amount of  $\text{H}_2\text{O}_2$  was dropped with agitation. And a dark yellow suspension was formed. The resultant was centrifuged and washed several times with 5% HCl aqueous solution and further with deionized water to remove impurities. Finally, the obtained slurry was kept in low temperature for further use.

## 2.3 Synthesis of $\text{Fe}_3\text{O}_4$ , $\text{Fe}_3\text{O}_4/\text{GO}$ , and $\text{Fe}_{3-x}\text{Cu}_x\text{O}_4/\text{GO}$ Nanocomposites

The  $\text{Fe}_3\text{O}_4$  NPs were prepared by a modified coprecipitation method. The detail steps were as follows: Firstly, 350 mL of deionized water was added into a 500-mL round-bottom flask that was kept in a preheated water bath (80 °C); secondly, 0.664 g of  $\text{FeCl}_2 \cdot 4\text{H}_2\text{O}$  and 1.751 g of  $\text{FeCl}_3 \cdot 6\text{H}_2\text{O}$  were added into the deionized water with stirring under  $\text{N}_2$  atmosphere; thirdly, 3 M NaOH solution was dropwise added into the mixture until the pH value reached to 9~10, and black precipitate was produced instantly; fourthly, the reactant was further stirred at 80 °C for 4 h; fifthly, the  $\text{Fe}_3\text{O}_4$  sample was collected with a magnet and washed several times with deionized water and anhydrous ethanol; finally, the sample was dried in a vacuum oven at 60 °C for 12 h.

The  $\text{Fe}_3\text{O}_4/\text{GO}$  nanocomposites were prepared according to the above processes except that the obtained GO was added into deionized water with agitation in the first step and further sonicated for 30 min. A series of the

$\text{Fe}_3\text{O}_4/\text{GO}$  nanocomposites were prepared according to the GO dosages. The preparation of the  $\text{Fe}_{3-x}\text{Cu}_x\text{O}_4/\text{GO}$  nanocomposites was based on that of the  $\text{Fe}_3\text{O}_4/\text{GO}$ . The only difference was that a certain amount of  $\text{CuCl}_2 \cdot 4\text{H}_2\text{O}$  was added to the previous system. And a series of the  $\text{Fe}_{3-x}\text{Cu}_x\text{O}_4/\text{GO}$  ( $x = 0, 0.025, 0.05, 0.075,$  and 0.1) nanocomposites were prepared.

## 2.4 Characterization

The crystal structures of the samples were characterized by X-ray powder diffractometer (XRD, Rigaku D/max-2400, Japan) with a  $\text{Cu K}\alpha$  radiation source. The morphologies of the samples were analyzed by high-resolution transmission electron microscope (HRTEM, JEOL JEM2100, Japan). The  $\text{N}_2$  adsorption-desorption isotherms of the samples were conducted at -196 °C (JW-BK100, China). The specific surface area (SSA) and pore size distribution were calculated by Brunauer-Emmett-Teller method and Barrelet-Juyner-Halenda (BJH) method, respectively. The surface states of the samples were identified by X-ray photoelectron spectroscopy (XPS, Thermo Scientific ESCALAB 250 XI, America). The surface functional groups of the samples were detected by Fourier transform-infrared spectroscopy (FT-IR, Thermo Scientific NICOLET 6700, America).

The p-NP concentration was measured by UV-Vis spectroscopy (YU-1810, Beijing Purikinje General Co., China) at wavelength of 400 nm. The chemical oxygen demand (COD) was analyzed by dichromate method (Tian et al. 2017). The concentrations of the total dissolved Fe and  $\text{Fe}^{2+}$  were tested by 1,10-phenantroline spectrophotometric method (Wan et al. 2016). And the  $\text{H}_2\text{O}_2$  concentration in aqueous solution was quantified by UV-Vis spectroscopy with titanium oxalate at wavelength of 395 nm (Tian et al. 2017).

## 2.5 Catalytic Activity Measurement

The catalytic performance of these samples was evaluated using p-NP as a model pollutant in aqueous solution. The experiments were conducted in a 150-mL conical flask with agitation. The detail experimental process was as follows: first, 0.1 g of the catalyst sample ( $\text{Fe}_3\text{O}_4$ ,  $\text{Fe}_3\text{O}_4/\text{GO}$ , or  $\text{Fe}_{3-x}\text{Cu}_x\text{O}_4/\text{GO}$  catalyst) was added into 100 mL of the simulated p-NP wastewater ( $100 \text{ mg L}^{-1}$ ), and the initial pH value was adjusted to 3.0 by  $\text{H}_2\text{SO}_4$  or NaOH

solution (1 M); then, 10 mmol L<sup>-1</sup> of H<sub>2</sub>O<sub>2</sub> was added with agitation for p-NP degradation. After some time, about 5 mL of the solution was taken out for analysis. Furthermore, the catalyst's reusability was also evaluated. The used catalyst was collected with an external magnet, and repeatedly washed with deionized water and ethanol for three times. After dried in vacuum oven, the catalyst was used for the next cycle under the same condition. All the experiments were repeated at least two times.

### 3 Results and Discussions

#### 3.1 Characterization of the Samples

Figure 1 shows the XRD patterns of the samples. The characteristic peak of the GOs appears at about 12.5° of 2θ (Guo et al. 2013). The diffraction peaks of the pure Fe<sub>3</sub>O<sub>4</sub> locate at 2θ of about 18.1°, 30.2°, 35.5°, 43.2°, 53.8°, 57.2°, and 62.8° that are indexed to (111), (220), (311), (400), (422), (511), and (440) lattice planes of Fe<sub>3</sub>O<sub>4</sub> with a cubic spinel structure according to the standard JCPDS data (Card No. 19-0629). For the as-prepared Fe<sub>3</sub>O<sub>4</sub>/GO, no obvious diffraction peaks of the GOs were observed. The reasons may be the following: (1)

small amounts of GOs in the nanocomposites (3.22 wt.%, 6.25 wt.%, and 9.09 wt.%), (2) much weaker diffraction intensity of GOs than that of Fe<sub>3</sub>O<sub>4</sub> NPs, and (3) well dispersion of Fe<sub>3</sub>O<sub>4</sub> NPs on GO sheets (Guo et al. 2013). Compared with Fe<sub>3</sub>O<sub>4</sub>/GO, the NPs in the Fe<sub>3-x</sub>Cu<sub>x</sub>O<sub>4</sub>/GO have relatively wider diffraction peaks, which may be originating from their smaller sizes (He et al. 2013; Bahadur et al. 2017).

The TEM images of these nanocomposites and corresponding NP size-distribution histograms are shown in Fig. 2. More than 200 of the nanoparticles for each sample were measured for the statistical analysis. The Fe<sub>3</sub>O<sub>4</sub>/GO (6.25 wt.%) sample has a large number of the Fe<sub>3</sub>O<sub>4</sub> aggregates. For the Cu-doped nanocomposites, the nanoparticle aggregations obviously decrease. The mean nanoparticle sizes of the nanocomposites are about 9.84 nm (Fe<sub>3</sub>O<sub>4</sub>/GO), 7.39 nm (Fe<sub>2.975</sub>Cu<sub>0.025</sub>O<sub>4</sub>/GO), 4.46 nm (Fe<sub>2.95</sub>Cu<sub>0.05</sub>O<sub>4</sub>/GO), 7.75 nm (Fe<sub>2.925</sub>Cu<sub>0.075</sub>O<sub>4</sub>/GO), and 6.68 nm (Fe<sub>2.9</sub>Cu<sub>0.1</sub>O<sub>4</sub>/GO), respectively. Compared with Fe<sup>2+</sup> ions, Cu<sup>2+</sup> ions have better inclination for the octahedral positions and smaller ionic radius (0.73 Å for Cu<sup>2+</sup> and 0.78 Å for Fe<sup>2+</sup> in octahedral coordination) (Barros et al. 2016). It may lead to the difference in average particle size.

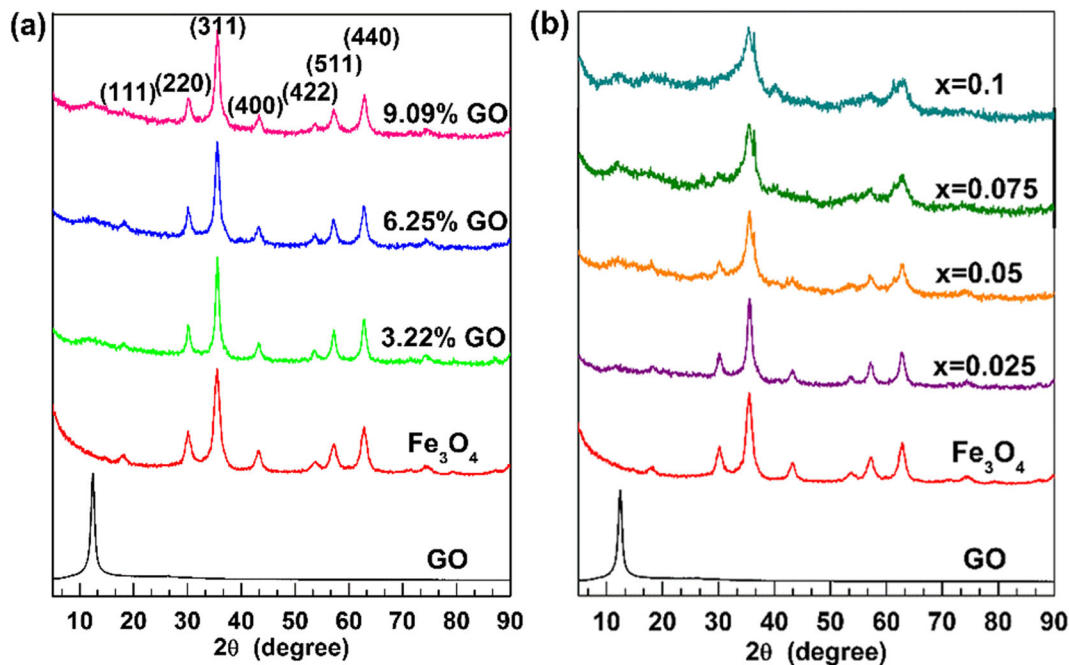
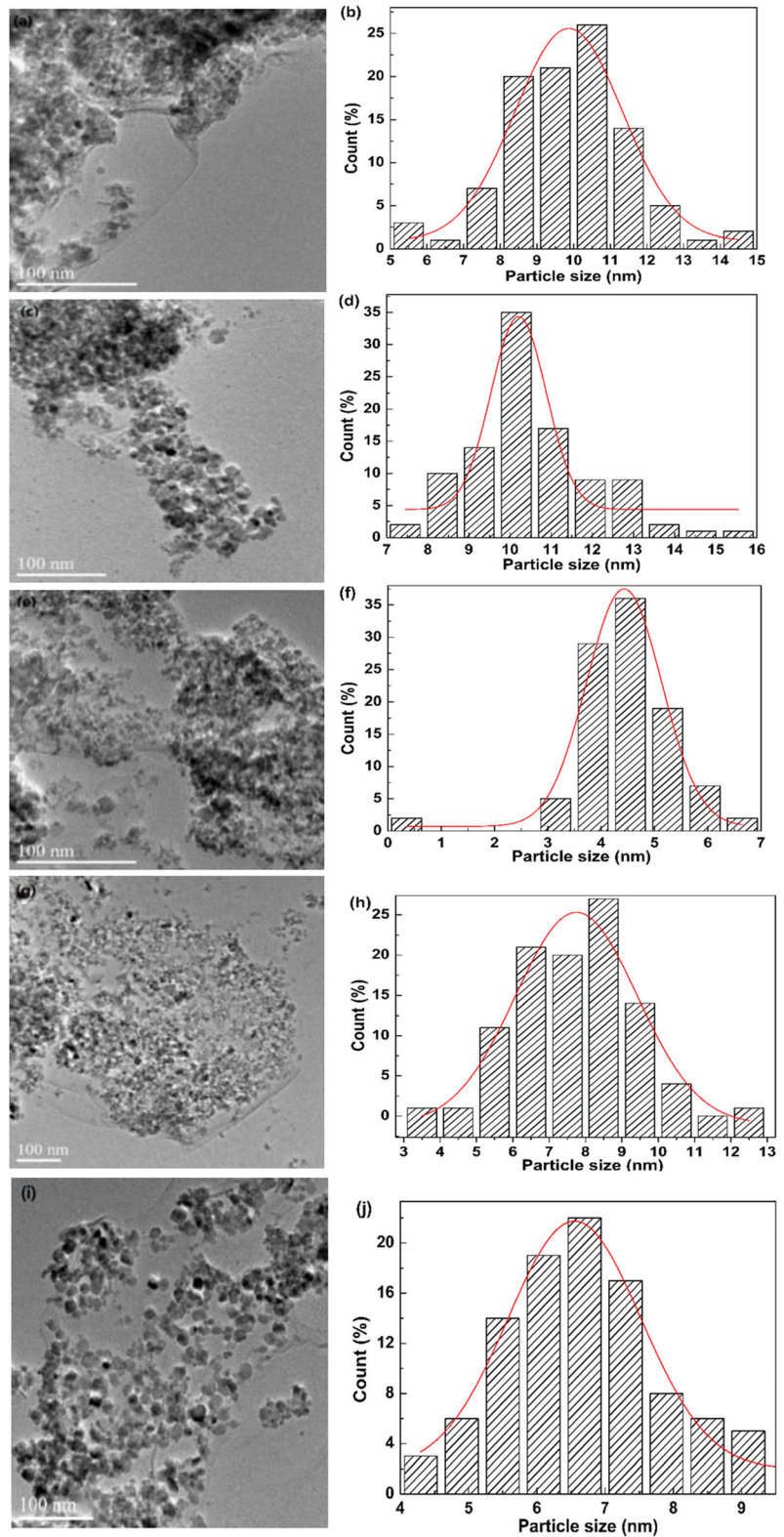


**Fig. 1** XRD patterns of **a** GO, Fe<sub>3</sub>O<sub>4</sub> NPs, and Fe<sub>3</sub>O<sub>4</sub>/GO nanocomposites and **b** Fe<sub>3-x</sub>Cu<sub>x</sub>O<sub>4</sub>/GO nanocomposites

**Fig. 2** TEM images of nanocomposites and their corresponding particle size distribution histograms. **a, b**  $\text{Fe}_3\text{O}_4/\text{GO}$  (6.25 wt.%). **c, d**  $\text{Fe}_3\text{-}_x\text{Cu}_x\text{O}_4/\text{GO}$  ( $x = 0.025$ ). **e, f**  $\text{Fe}_3\text{-}_x\text{Cu}_x\text{O}_4/\text{GO}$  ( $x = 0.05$ ). **g, h**  $\text{Fe}_3\text{-}_x\text{Cu}_x\text{O}_4/\text{GO}$  ( $x = 0.075$ ). **i, j**  $\text{Fe}_3\text{-}_x\text{Cu}_x\text{O}_4/\text{GO}$  ( $x = 0.1$ )



The  $N_2$  adsorption–desorption isotherms of the  $Fe_{3-x}Cu_xO_4/GO$  nanocomposites are shown in Fig. S1. And the corresponding SSAs and pore structure parameters are listed in Table S1. It can be seen that the SSAs of the composites become higher with increasing of the GO content that may be the large SSA of the GOs. The SSAs of the nanocomposites become high after Cu doping. The corresponding SSAs increase from  $137.2 \text{ m}^2 \text{ g}^{-1}$  ( $Fe_3O_4/GO$ ) to  $142.0 \text{ m}^2 \text{ g}^{-1}$  ( $Fe_{3-x}Cu_xO_4/GO$ ,  $x = 0.025$ ),  $220.5 \text{ m}^2 \text{ g}^{-1}$  ( $x = 0.05$ ),  $223.9 \text{ m}^2 \text{ g}^{-1}$  ( $x = 0.075$ ), and  $224.0 \text{ m}^2 \text{ g}^{-1}$  ( $x = 0.1$ ), respectively. Those data may reflect the states of the catalysts to some extent that the Cu-doped nanocomposites have less aggregates comparing with  $Fe_3O_4/GO$ .

The XPS analysis was used to study the surface states of the nanocomposites before and after use. As shown in Fig. S2 (a)(d), the XPS full survey spectra reveal that the  $Fe_{2.925}Cu_{0.075}O_4/GO$  contain C, O, Fe, and Cu elements (binding energy, 283.5 (C1s); 529.1 (O1s); 709.8 (Fe2p); and 932.7 eV (Cu2p), respectively). For the original  $Fe_{2.925}Cu_{0.075}O_4/GO$ , the binding energy values at 710.1 and 712.0 eV or 717.5 and 724.3 eV indicate the presence of  $Fe^{2+}$  and  $Fe^{3+}$ , respectively. And the binding energy of Cu2p3/2 and Cu2p1/2 are located at 932.3 and 933.6 eV, respectively (Barros et al. 2016). For the used  $Fe_{2.925}Cu_{0.075}O_4/GO$ , the Fe2p peaks appear at 710.0 and 711.7 eV or 717.4 and 724.2 eV, respectively. However, there is no obvious peak of Cu2p as shown in Fig. S2 (f). This result indicates the significant wastage of the Cu element in Fenton reaction.

The FT-IR spectra of p-NP and  $Fe_{2.925}Cu_{0.075}O_4/GO$  before and after four reuses are shown in Fig. S3 (a) and (b), respectively. Compared with the raw  $Fe_{2.925}Cu_{0.075}O_4/GO$ , there are some changes for the used sample. The peaks belonging to O–H, C–H, C=C, C–O, and C=O functional groups have some slight differences. The peaks of these functional groups are red shifted and sharpened, especially for of the aromatic C=C bonding. And two new peaks at 1101 and  $1404 \text{ cm}^{-1}$  appear in the FT-IR spectrum of the used catalyst, which may be contributed to the intermediate organic molecules originating from the p-NP degradation. Furthermore, the peaks at 584 and  $578 \text{ cm}^{-1}$  can be attributed to Fe–O in  $Fe_3O_4$ , suggesting the connection of  $Fe_3O_4$  with the –COO– functional group on the edge of the GO sheets (Guo

et al. 2013), which is consistent with the results of TEM analysis.

### 3.2 Effects of Parameters on the Degradation of p-NP

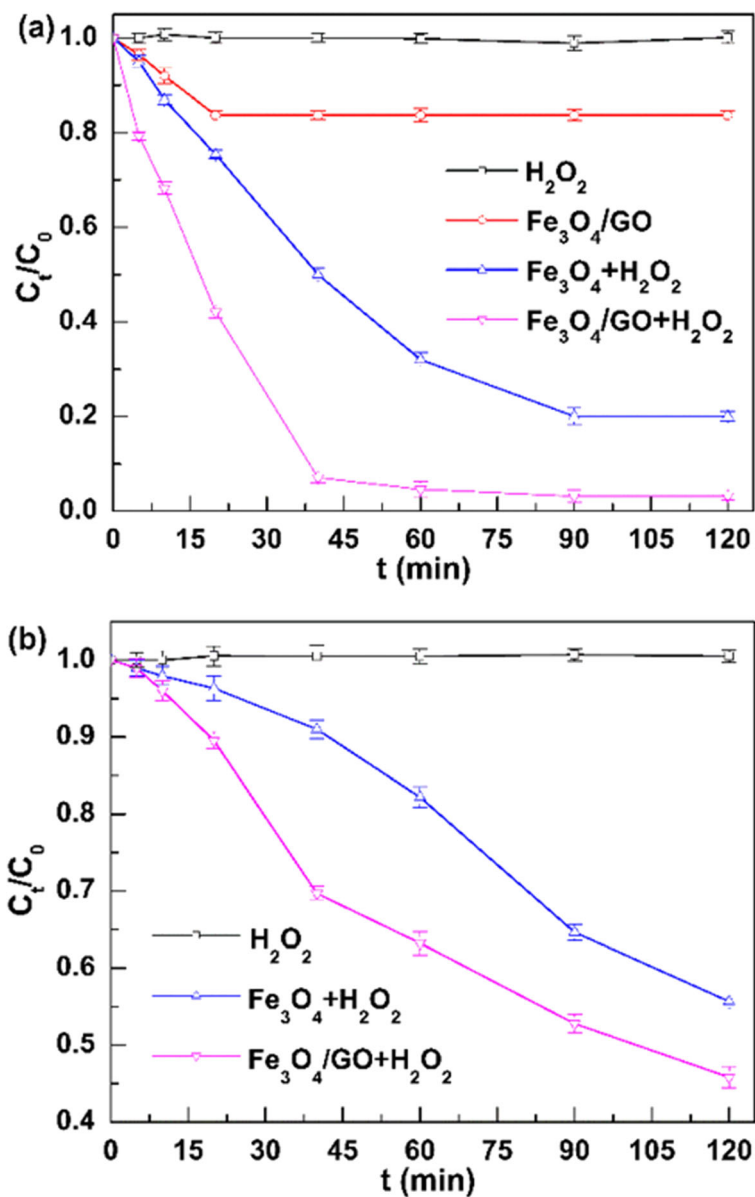
#### 3.2.1 Effect of Catalysts on Degradation of p-NP

The catalytic activity of as-prepared catalysts is evaluated using p-NP as the stimulated pollutant in aqueous solution (30 °C of temperature, 3.0 of pH value,  $100 \text{ mg L}^{-1}$  of p-NP concentration,  $1.0 \text{ g L}^{-1}$  of catalyst dosage, and  $10 \text{ mmol L}^{-1}$  of  $H_2O_2$  concentration). When only  $H_2O_2$  is added without catalyst in the reaction system, the p-NP removal efficiency is just only 1.12% as shown in Fig. 3a. It indicates a weak oxidizing ability of  $H_2O_2$  to p-NP molecular. The p-NP removal efficiency is also as low as 16.3% for  $Fe_3O_4/GO$  without  $H_2O_2$ , which may be the composite's absorption. When  $Fe_3O_4-H_2O_2$  or  $Fe_3O_4/GO-H_2O_2$  system is used, the p-NP removal efficiency reaches to 80% and 96.9% in 120 min, respectively. It is the generation of reactive species ( $\cdot OH$ ) ( $E_0 = 2.8 \text{ V}$ ). Figure 3b shows the  $H_2O_2$  consumption with the treatment time.  $H_2O_2$  is almost never consumed without catalyst. After adding  $Fe_3O_4$  or  $Fe_3O_4/GO$ , the  $H_2O_2$  consumption rates are about 44.3% and 54.1% in 120 min, respectively.

#### 3.2.2 Effect of GO Contents on Degradation of p-NP

Figure 4a shows the effect of the GO contents in  $Fe_3O_4/GO$  on the p-NP degradation. With increasing of the GO content from 0 to 6.25 wt.%, the p-NP removal rate increases from about 80 to 96.9%. The reasons may be the following: (1) agglomeration reduction of  $Fe_3O_4$  NPs due to GO support and (2) synergistic effect between GO and  $Fe_3O_4$  NPs (Zubir et al. 2014; Yu et al. 2016). But when the GO content increases to about 9.09 wt.%, the p-NP removal efficiency reduces to 88.3%. The following are possible: 1) re-stacking of some GO sheets through the p–p interactions and (2) covering the catalytic sites of  $Fe_3O_4$  NPs by superfluous GOs. Usually, in a certain range, the more  $Fe_3O_4$  exists, the more  $H_2O_2$  will be consumed and the higher the p-NP degradation efficiency will be achieved. However, if the GO content is too low or too high, the synergistic effect between the two components will become weak (He et al. 2013). Figure. 4b indicates the effect of the GO content on the  $H_2O_2$  consumption rate. It is clear that the  $H_2O_2$  consumption rate is relatively higher for

**Fig. 3** Effect of catalysts on **a** p-NP removal efficiency and **b** H<sub>2</sub>O<sub>2</sub> decomposition



6.25 wt.% of the GO content in our research system. The reaction could be considered as a pseudo-first-order. And the pseudo-first-order rate constant (*k*) is calculated according to Eq. (1) (Wang 2008; Wang et al. 2017a, b):

$$\ln(C_t/C_0) = -kt \tag{1}$$

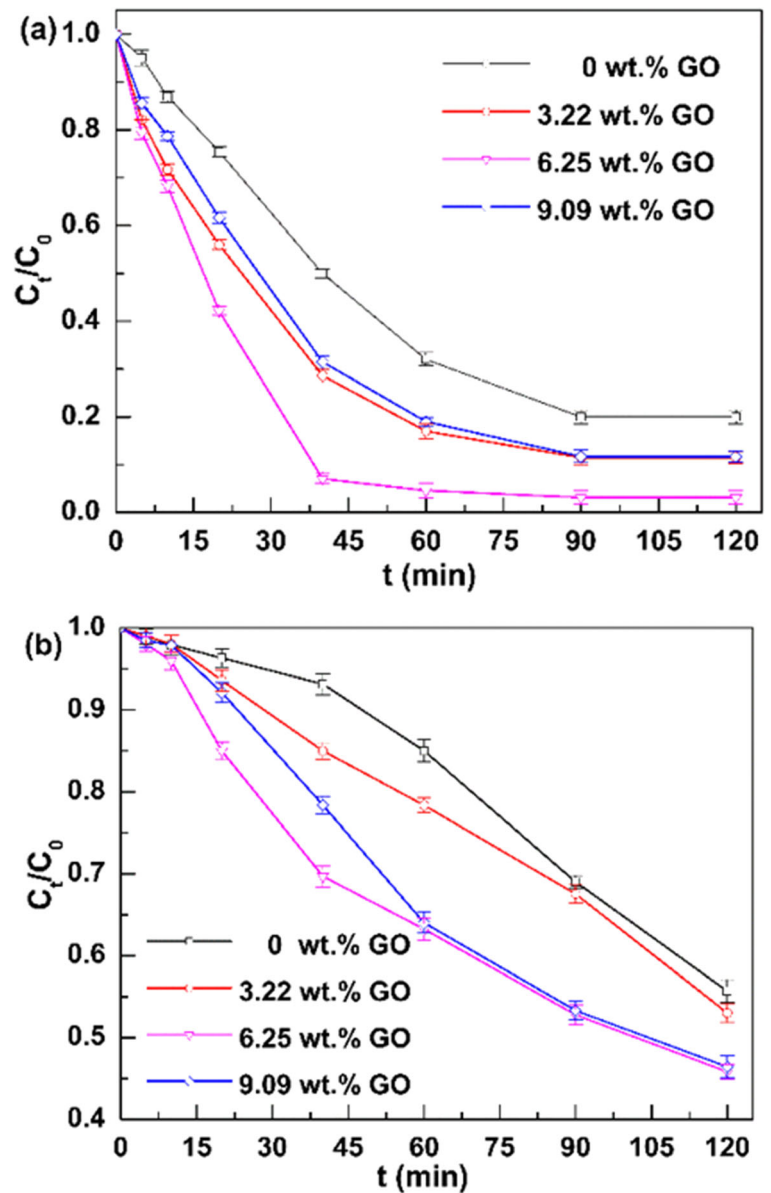
where, *C<sub>t</sub>* is the p-NP concentration at reaction time *t* (mg/L); *C<sub>0</sub>* is the initial p-NP concentration (mg/L), and *C* is a constant. The obtained data are listed in Table 1. The rate constants of the catalysts with different GO

contents (0, 3.22, 6.25, and 9.09 wt.%) are 0.0186, 0.0250, 0.0427, and 0.0249 min<sup>-1</sup>, respectively. The data demonstrate that the catalyst with 6.25 wt.% of GO content has highest catalytic ability among the above said samples.

### 3.2.3 Effect of Cu Doping on Degradation of p-NP

Further, the effects of Cu doping in the catalyst on the p-NP degradation were studied. As shown in Fig. 5a, the p-NP degradation rates obviously become fast after the

**Fig. 4** Effect of GO content on **a** p-NP removal efficiency and **b**  $H_2O_2$  decomposition



Cu doping. The p-NP removal efficiencies of all the Cu doped catalysts exceed 95.0% in 20 min, while that of

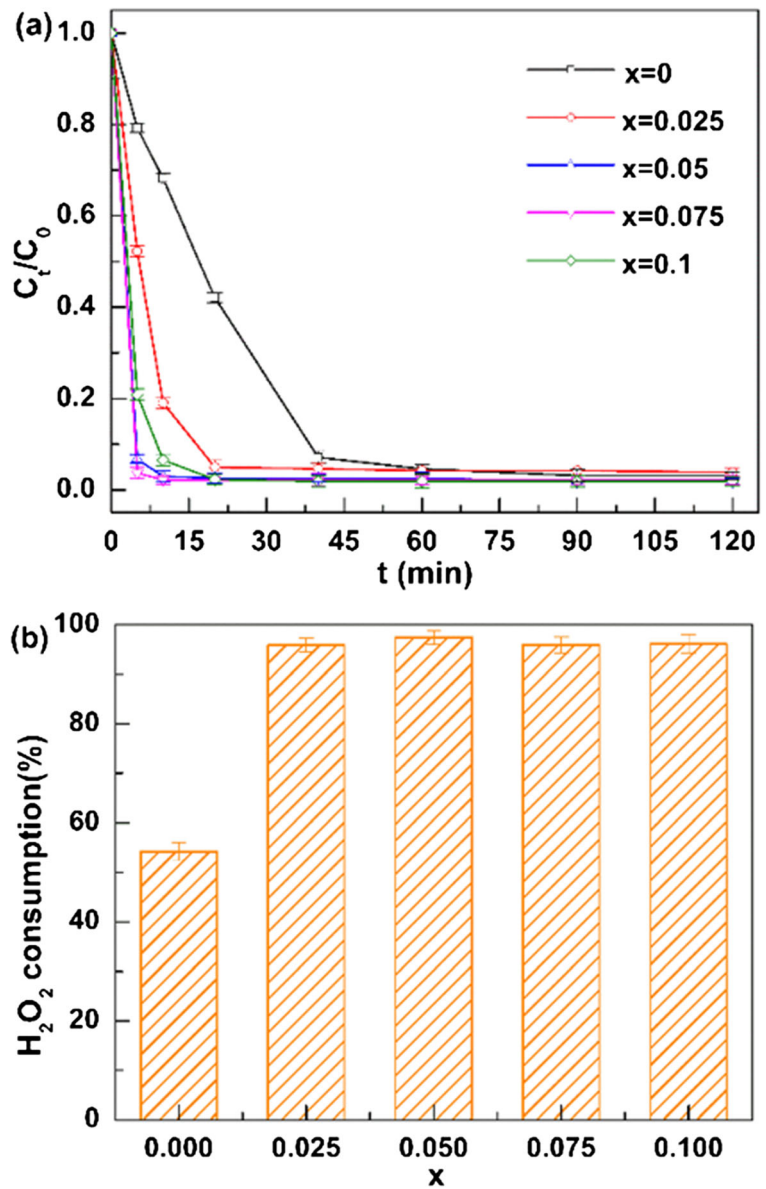
**Table 1** Calculated pseudo-first-order rate constant of samples

Samples	$k$ ( $\text{min}^{-1}$ )	$R^2$
0 wt.% GO	0.0186	0.995
3.22 wt.% GO	0.0250	0.972
6.25 wt.% GO	0.0427	0.896
9.09 wt.% GO	0.0249	0.984

the  $Fe_3O_4/GO$  catalyst is only 57.9%. With increasing the Cu content, the p-NP removal efficiency in 20 min increases and reaches a maximal value at 0.075 of  $x$  value. It may be that more  $Cu^{2+}$  ions replace  $Fe^{2+}$  ions in the octahedral sites and decrease the Fe-active sites. Compared with the  $Fe_3O_4/GO$  catalyst, the  $H_2O_2$  consumptions of the  $Fe_{3-x}Cu_xO_4/GO$  catalysts increase significantly as shown in Fig. 5b. But the  $H_2O_2$  utilization efficiency will decrease for the catalyst with excessive Cu doping content. The results show that appropriate Cu doping in the catalyst is conducive to the improvement



**Fig. 5** Effect of Cu doping on **a** p-NP degradation and **b** H<sub>2</sub>O<sub>2</sub> decomposition



of the catalytic properties. In the following studies, the Fe<sub>2.925</sub>Cu<sub>0.075</sub>O<sub>4</sub>/GO catalyst was used.

### 3.2.4 Effect of the Catalyst Dosage on Degradation of p-NP

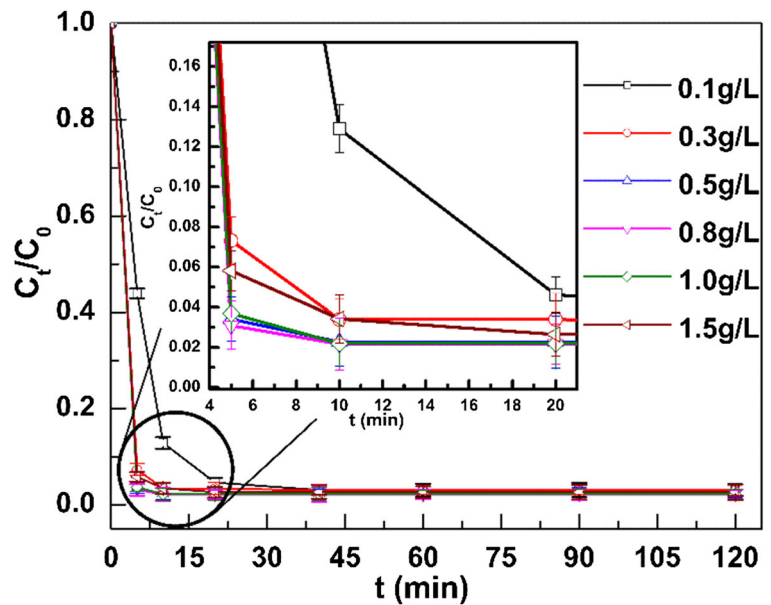
The effect of catalyst dosage on the p-NP degradation was further studied (100 mg L<sup>-1</sup> of initial p-NP concentration, 10 mmol L<sup>-1</sup> of H<sub>2</sub>O<sub>2</sub> concentration, 3.0 of pH value, and 30 °C of temperature). Figure 6 displays the effect of the catalyst dosage on the p-NP degradation efficiency. As the catalyst dosage increases from 0.1 to

1.5 g L<sup>-1</sup>, the p-NP removal rate increases and reaches to a maximal value (97.8%) at 0.8 g L<sup>-1</sup> of the catalyst dosage, and then slightly decreases. The catalyst agglomeration is possible. Despite this, the p-NP degradation efficiencies still exceed 96.0%. Therefore, the following experiments are carried out at 0.8 g L<sup>-1</sup> of the catalyst dose.

### 3.2.5 Effect of Initial pH on Degradation of p-NP

The pH value is an important parameter in wastewater treatment. Although Fe<sup>2+</sup> remains in dissolved form

**Fig. 6** Effect of catalyst dosage on p-NP degradation



even at neutral condition,  $\text{Fe}^{3+}$  will form ferric hydroxide sludge if the pH value is larger than 4. Thus, a strict acidic condition ( $\text{pH} < 4$ ) is usually required for practical applications (Bokare and Choi 2014).  $\text{Fe}(\text{OH})^+$  will form at low pH value (2–4) and may have higher active catalytic activity than  $\text{Fe}^{2+}$  in Fenton reaction (Malik and Saha 2003; Wang 2008). So, the experimental conditions are as follows:  $100 \text{ mg L}^{-1}$  of initial p-NP concentration,  $0.8 \text{ g L}^{-1}$  of catalyst dosage,  $10 \text{ mmol L}^{-1}$  of  $\text{H}_2\text{O}_2$  concentration, and  $30^\circ\text{C}$  of temperature and 2–3.5 of pH value. It can be seen from Fig. 7 that the p-NP removal efficiencies all exceed 97% in 10 min in 2.0 to 3.0 of pH value. When the pH value is 3.5, the removal efficiency decreases to about 90.0% in 120 min. Therefore, the relatively optimal pH value is about 3.0 in our researched scope.

### 3.2.6 Effect of $\text{H}_2\text{O}_2$ Concentration on Degradation of p-NP

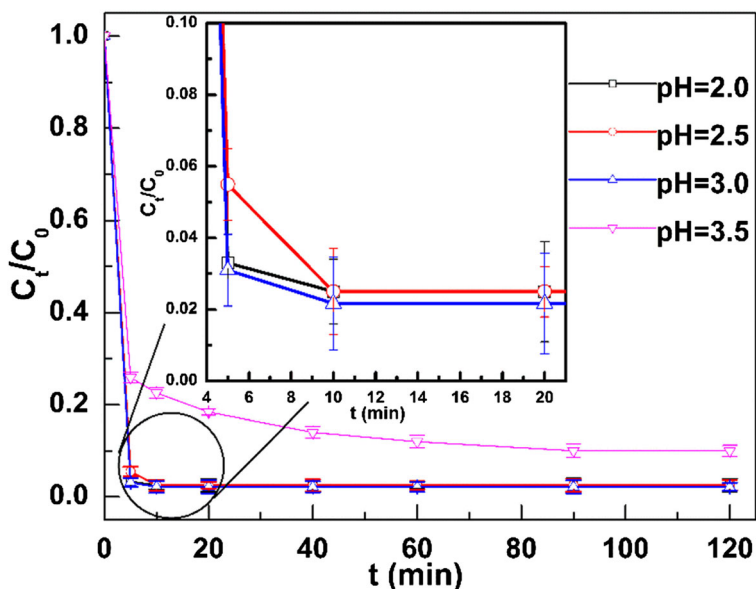
Following, the effect of  $\text{H}_2\text{O}_2$  concentration on p-NP degradation was also investigated (an initial p-NP concentration of  $100 \text{ mg L}^{-1}$ , a catalyst dosage of  $0.8 \text{ g L}^{-1}$ , pH value of 3.0, and temperature of  $30^\circ\text{C}$ ). As shown in Fig. 8, the p-NP conversion and COD removal efficiencies increase with increasing of the  $\text{H}_2\text{O}_2$  concentration and reach to the maximal values (98.4% and 74.7%) at  $15 \text{ mmol L}^{-1}$ . When the concentration is as high as  $20 \text{ mmol L}^{-1}$ , there is no obvious enhancement of the

p-NP degradation and COD removal efficiency. Excessive  $\text{H}_2\text{O}_2$  can lead an unprofitable  $\text{H}_2\text{O}_2$  consumption in the Fenton process. Therefore, subsequent experiments are conducted at  $15 \text{ mmol L}^{-1}$  of the  $\text{H}_2\text{O}_2$  concentration.

### 3.3 Iron Leaching and $\text{H}_2\text{O}_2$ Decomposition

The iron leaching and  $\text{H}_2\text{O}_2$  consumption were also studied under the optimal reaction conditions ( $100 \text{ mg L}^{-1}$  of initial p-NP concentration,  $15 \text{ mmol L}^{-1}$  of  $\text{H}_2\text{O}_2$  concentration, 3.0 of pH, and  $30^\circ\text{C}$  of temperature). As shown in Fig. 9a, the concentration of total dissolved iron increases with prolonging the reaction time, and about  $11.0 \text{ mg L}^{-1}$  of dissolved iron is released into solution within 120 min. In the first 20 min, the concentrations of ferrous ion and total dissolved iron have a similar change trend. And ferrous ions account for the majority of total dissolved iron. It may be the transformation of  $\text{Fe}^{3+}$  into  $\text{Fe}^{2+}$  by  $\text{Cu}^+$ , which is benefit for reversible conversion between  $\text{Fe}^{2+}$  and  $\text{Fe}^{3+}$  in octahedron structure (Barros et al. 2016). The ferrous ion concentration increases rapidly in the first 20 min, which corresponds to the rapid p-NP degradation as shown in Fig. 9b. After 40 min, the  $\text{H}_2\text{O}_2$  consumption rate obviously decreases with the reduction of  $\text{Fe}^{2+}$  ion. The  $\text{H}_2\text{O}_2$  utilization efficiency ( $E$ ) is a very important index to evaluate the nanocomposite's catalytic ability (Gao et al. 2015). It is defined as the

**Fig. 7** Effect of initial pH on p-NP degradation

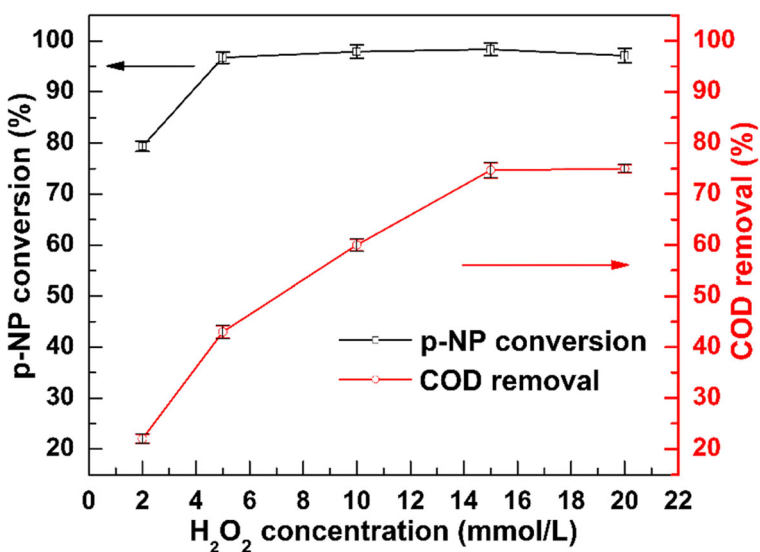


amount of removed COD corresponding to the consumption of the unit mass H<sub>2</sub>O<sub>2</sub> and calculated according to Eq. (2) (Wan et al. 2016):

$$E(\%) = \frac{\Delta[\text{COD}]}{0.47 \times \Delta[\text{H}_2\text{O}_2]} \times 100 \tag{2}$$

Where,  $\Delta[\text{COD}]$  is the removed COD value (mg L<sup>-1</sup>);  $\Delta[\text{H}_2\text{O}_2]$  is the decomposed H<sub>2</sub>O<sub>2</sub> amount in this process (mg L<sup>-1</sup>), and 0.47 is the conversion factor (Bokare and Choi 2014). Here,  $\Delta[\text{COD}]$  and  $\Delta[\text{H}_2\text{O}_2]$  were about 120 mg L<sup>-1</sup> and 484.5 mg L<sup>-1</sup>, respectively.

**Fig. 8** Effect of initial H<sub>2</sub>O<sub>2</sub> concentration on p-NP removal efficiency

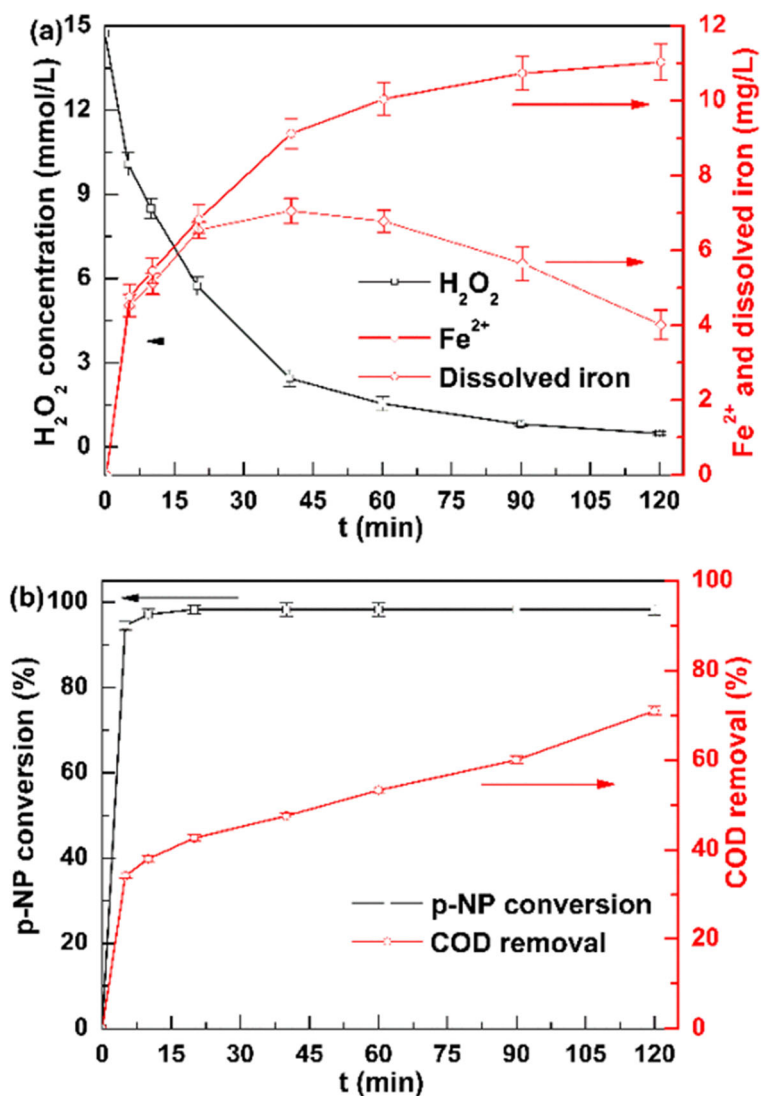


Therefore, the H<sub>2</sub>O<sub>2</sub> utilization efficiency is about 52.7%.

### 3.4 Stability and Reusability of the Catalyst

The stability and reusability of the Fe<sub>2.925</sub>Cu<sub>0.075</sub>O<sub>4</sub>/GO nanocomposite were also investigated. The experiments were carried out under the optimal condition in our research range (100 mg L<sup>-1</sup> of initial p-NP concentration, 0.8 g L<sup>-1</sup> of catalyst dosage, 15 mmol L<sup>-1</sup> of initial H<sub>2</sub>O<sub>2</sub> concentration, 3.0 of pH, and 30 °C of temperature). Figure 10 shows that the p-NP degradation

**Fig. 9** **a**  $\text{H}_2\text{O}_2$  decomposition, iron dissolution, and **b** p-NP conversion and COD removal during p-NP degradation under the optimum reaction conditions



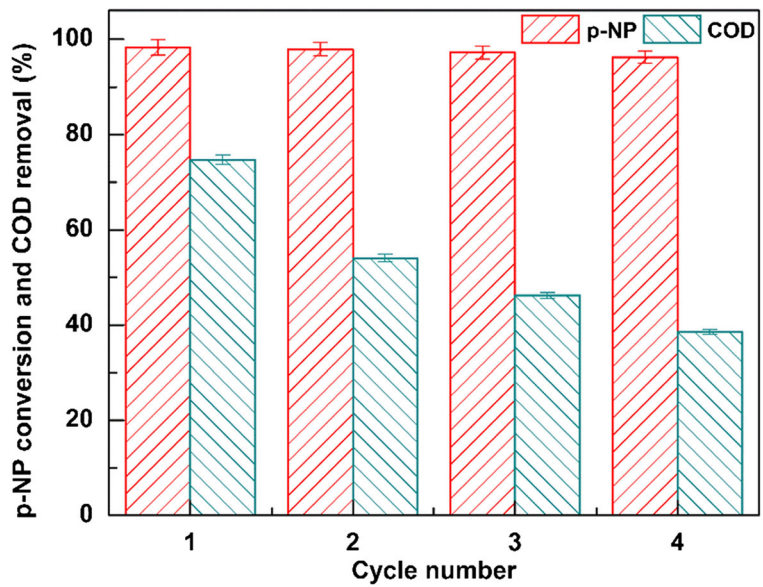
efficiency is still more than 96.0% after four recycles. However, the corresponding COD removal efficiency drops from 74.7 to only 38.7%. It is possible the Cu wastage in nanocomposite. Figure S4 displays that the  $\text{Fe}_{2.925}\text{Cu}_{0.075}\text{O}_4/\text{GO}$  nanocomposite could be easily separated with an external magnet from water. It is very important for practical application.

### 3.5 Catalytic Mechanism of $\text{Fe}_{2.925}\text{Cu}_{0.075}\text{O}_4/\text{GO}$ Nanocomposite on p-NP Degradation

The possible mechanism of the p-NP degradation in  $\text{Fe}_{2.925}\text{Cu}_{0.075}\text{O}_4/\text{GO}-\text{H}_2\text{O}_2$  system is shown in Fig. 11. Firstly,  $\text{H}_2\text{O}_2$  adsorbed on the surface of

nanocomposite due to synergistic adsorption of  $\text{Fe}_{2.925}\text{Cu}_{0.075}\text{O}_4$  NPs and GOs. Then,  $\text{H}_2\text{O}_2$  was transformed into  $\cdot\text{OH}$  and  $\text{OH}^-$  on the Fe-active and Cu-active sites by Eqs. (3) and (4). And  $\text{Fe}^{3+}$  and  $\text{Cu}^{2+}$  reacted with  $\text{H}_2\text{O}_2$  to form  $\text{Fe}^{2+}$ ,  $\text{Cu}^+$ , and  $\cdot\text{OOH}$  (Eqs. (5) and (6)). And the synergistic effect between Fe and Cu ions in the octahedral sites of the spinel structure promoted the production of  $\cdot\text{OH}$ .  $\text{Cu}^+$  could react with  $\text{Fe}^{3+}$  to regenerate  $\text{Fe}^{2+}$  (Eq. (7)), which could accelerate the conversion of  $\text{Fe}^{3+}$  into  $\text{Fe}^{2+}$ . The Cu doping plays a positive role in the enhancement of the p-NP degradation efficiency. Furthermore, GO may accelerate electron transmission and  $\text{H}_2\text{O}_2$  absorption during the reactions. The

**Fig. 10** Reusability of  $\text{Fe}_{2.925}\text{Cu}_{0.075}\text{O}_4/\text{GO}$  nanocomposite



formed  $\cdot\text{OH}$  reacted with p-NP molecular and its intermediate products (Eqs. (8) and (9)).

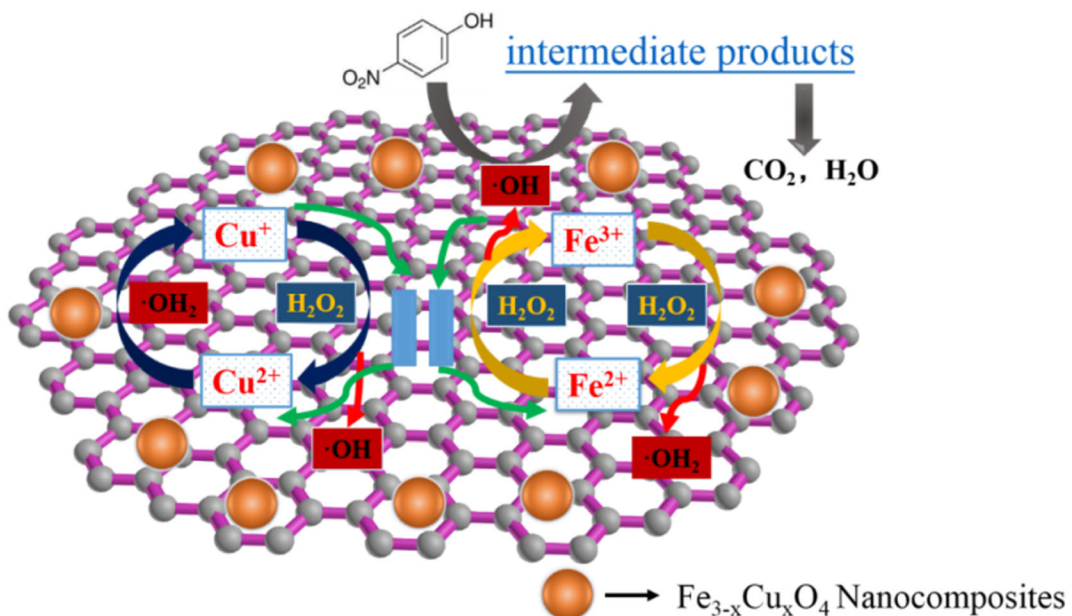
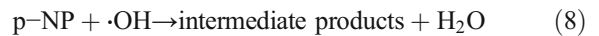
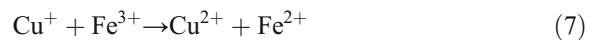


**Fig. 11** Possible mechanism of p-NP degradation in heterogeneous  $\text{Fe}_{2.925}\text{Cu}_{0.075}\text{O}_4/\text{GO}-\text{H}_2\text{O}_2$  system

## 4 Conclusion

The Fe<sub>3</sub>O<sub>4</sub>/GO and Fe<sub>3-x</sub>Cu<sub>x</sub>O<sub>4</sub>/GO (0 ≤ x ≤ 0.1) nanocomposites were prepared by a co-precipitation method and used as heterogeneous Fenton catalyst for the p-NP degradation. The Fe<sub>3</sub>O<sub>4</sub>/GO containing 6.25 wt.% of GO has the best catalytic properties among the samples with different GO contents. The catalytic performances of the nanocomposites were remarkably improved after doping Cu, especially for Fe<sub>2.925</sub>Cu<sub>0.075</sub>O<sub>4</sub>/GO. The p-NP degradation rate in 20 min for Fe<sub>2.925</sub>Cu<sub>0.075</sub>O<sub>4</sub>/GO is about 97.8%, while that for Fe<sub>3</sub>O<sub>4</sub>/GO is only 57.9% at the same reaction condition. Under the optimal reaction condition, the p-NP conversion and COD removal efficiencies for Fe<sub>2.925</sub>Cu<sub>0.075</sub>O<sub>4</sub>/GO are 98.4% and 74.7%, respectively. The corresponding H<sub>2</sub>O<sub>2</sub> decomposition reaches to 96.7%. The p-NP removal rate for Fe<sub>2.925</sub>Cu<sub>0.075</sub>O<sub>4</sub>/GO is still as high as 96.0% after four reuse, while the COD removal rate gradually decreases. We believe that the Fe<sub>2.925</sub>Cu<sub>0.075</sub>O<sub>4</sub>/GO catalyst is a promising heterogeneous Fenton catalyst in phenolic wastewater treatment. The synergetic catalytic effect is the key for the high COD removal rate. But how to immobilize the Cu ingredient in the nanocomposite is a very important work in the next work.

**Funding Information** This study is financially supported by the National Natural Science Foundation of China (Grant Nos. 21174011 and U1462102).

### Compliance with Ethical Standards

**Conflict of Interest** The authors declare that they have no conflicts of interest.

**Publisher's Note** Springer Nature remains neutral with regard to jurisdictional claims in published maps and institutional affiliations.

## References

Bahadur, A., Saeed, A., Shoaib, M., Lqbal, S., Bashir, M. I., Waqas, M., Hussain, M. N., & Abbas, N. (2017). Eco-friendly synthesis of magnetite (Fe<sub>3</sub>O<sub>4</sub>) nanoparticles with tunable size: Dielectric, magnetic, thermal and optical studies. *Materials Chemistry & Physics*, *198*, 229–235.

Barros, W. R. P., Steter, J. R., Lanza, M. R. V., & Tavares, A. C. (2016). Catalytic activity of Fe<sub>3-x</sub>Cu<sub>x</sub>O<sub>4</sub>, (0 ≤ x ≤ 0.25) nanoparticles for the degradation of Amaranth food dye by

heterogeneous electro-Fenton process. *Applied Catalysis B Environmental*, *180*, 434–441.

Bokare, A. D., & Choi, W. Y. (2014). Review of iron-free Fenton-like systems for activating H<sub>2</sub>O<sub>2</sub> in advanced oxidation processes. *Journal of Hazardous Materials*, *275*, 121–135.

Chen, H. H., Yang, M., Tao, S., & Chen, G. W. (2017). Oxygen vacancy enhanced catalytic activity of reduced Co<sub>3</sub>O<sub>4</sub> towards p-nitrophenol reduction. *Applied Catalysis B Environmental*, *209*, 648–656.

Costa, R. C., Lelis, M. F., Oliveira, L. C., Fabris, J. D., Ardisson, J. D., Rios, R. R., Silva, C. N., & Lago, R. M. (2006). Novel active heterogeneous Fenton system based on Fe<sub>3-x</sub>M<sub>x</sub>O<sub>4</sub> (Fe, Co, Mn, Ni): The role of M<sup>2+</sup> species on the reactivity towards H<sub>2</sub>O<sub>2</sub> reactions. *Journal of Hazardous Materials*, *129*, 171–178.

Gao, Y. W., Wang, Y., & Zhang, H. (2015). Removal of rhodamine B with Fe-supported bentonite as heterogeneous photo-Fenton catalyst under visible irradiation. *Applied Catalysis B Environmental*, *178*, 29–36.

Gonzalez-Olmos, R., Martin, M. J., Georgi, A., Kopinke, F. D., Oller, I., & Malato, S. (2012). Fe-zeolites as heterogeneous catalysts in solar Fenton-like reactions at neutral pH. *Applied Catalysis B Environmental*, *125*(3), 51–58.

Guo, S., Zhang, G. K., Guo, Y. D., & Yu, J. C. (2013). Graphene oxide-Fe<sub>2</sub>O<sub>3</sub> hybrid material as highly efficient heterogeneous catalyst for degradation of organic contaminants. *Carbon*, *60*(14), 437–444.

He, G. Y., Liu, W. F., Sun, X. Q., Chen, Q., Wang, X., & Chen, H. Q. (2013). Fe<sub>3</sub>O<sub>4</sub>@graphene oxide composite: A magnetically separable and efficient catalyst for the reduction of nitroarenes. *Materials Research Bulletin*, *48*(5), 1885–1890.

Huang, H. H., Lu, M. C., & Chen, J. N. (2001). Catalytic decomposition of hydrogen peroxide and 2-chlorophenol with iron oxides. *Water Research*, *35*(9), 2291–2299.

Kakavandi, B., Takdastan, A., Jaafarzadeh, N., Azizi, M., Mirzaei, A., & Azari, A. (2016). Application of Fe<sub>3</sub>O<sub>4</sub>@C catalyzing heterogeneous UV-Fenton system for tetracycline removal with a focus on optimization by a response surface method. *Journal of Photochemistry & Photobiology A Chemistry*, *314*(1), 178–188.

Kwan, W. P., & Voelker, B. M. (2003). Rates of hydroxyl radical generation and organic compound oxidation in mineral-catalyzed Fenton-like systems. *Environ Science & Technology*, *37*(6), 1150–1158.

Magalhães, F., Pereira, M. C., Botrel, S. E. C., Fabris, J. D., Macedo, W. A., Mendonca, R., Lago, R. M., & Oliveira, L. C. A. (2007). Cr-containing magnetites Fe<sub>3-x</sub>Cr<sub>x</sub>O<sub>4</sub>: The role of Cr<sup>3+</sup> and Fe<sup>2+</sup> on the stability and reactivity towards H<sub>2</sub>O<sub>2</sub> reactions. *Applied Catalysis A General*, *332*(1), 115–123.

Malik, P. K., & Saha, S. K. (2003). Oxidation of direct dyes with hydrogen peroxide using ferrous ion as catalyst. *Separation and Purification Technology*, *31*, 241–250.

Matta, R., Hanna, K., & Chiron, S. (2007). Fenton-like oxidation of 2,4,6-trinitrotoluene using different iron minerals. *Science of the Total Environment*, *385*(1), 242–251.

Menini, L., Pereira, M. C., Parreira, L. A., Fabris, J. D., & Gusevskaya, E. V. (2008). Cobalt-and manganese-substituted ferrites as efficient single-site heterogeneous catalysts for aerobic oxidation of monoterpene alkenes under solvent-free conditions. *Journal of Catalysis*, *254*(2), 355–364.

- Moura, F. C., Araujo, M. H., Costa, R. C., Fabris, J. D., Ardisson, J. D., Macedo, W. A., & Lago, R. M. (2005). Efficient use of Fe metal as an electron transfer agent in a heterogeneous Fenton system based on  $\text{Fe}^0/\text{Fe}_3\text{O}_4$  composites. *Chemosphere*, *60*(8), 1118–1123.
- Nejad, M. A., & Jonsson, M. (2004). Reactivity of hydrogen peroxide towards  $\text{Fe}_3\text{O}_4$ ,  $\text{Fe}_2\text{CoO}_4$ , and  $\text{Fe}_2\text{NiO}_4$ . *Journal of Nuclear Materials*, *334*(1), 28–34.
- Pereira, M. C., Oliveira, L. C. A., & Murad, E. (2012). Iron oxide catalysts: Fenton and Fenton-like reactions—A review. *Clay Minerals*, *47*(3), 285–302.
- Pugazhenthiran, N., Sathishkumar, P., Murugesan, S., & Anandan, S. (2011). Effective degradation of acid orange 10 by catalytic ozonation in the presence of Au-Bi<sub>2</sub>O<sub>3</sub> nanoparticles. *Chemical Engineering Journal*, *168*(3), 1227–1233.
- Sun, L., & Fugetsu, B. (2013). Mass production of graphene oxide from expanded graphite. *Materials Letters*, *109*(1), 207–210.
- Tian, X. J., Liu, Y. F., Chi, W. D., Wang, Y., Yue, X. Z., Huang, Q. G., & Yu, C. Y. (2017). Catalytic degradation of phenol and p-Nitrophenol using  $\text{Fe}_3\text{O}_4/\text{MWCNT}$  nanocomposites as heterogeneous Fenton-like catalyst. *Water, Air, & Soil Pollution*, *228*, 297.
- Ullah, K., Ye, S., Zhu, L., Meng, Z. D., Sarkar, S., & Oh, W. C. (2014). Microwave assisted synthesis of a noble metal-graphene hybrid photocatalyst for high efficient decomposition of organic dyes under visible light. *Materials Science and Engineering B*, *180*, 20–26.
- Wan, D., Li, W. B., Wang, G. H., Lu, L. L., & Wei, X. B. (2016). Degradation of p-Nitrophenol using magnetic  $\text{Fe}^0/\text{Fe}_3\text{O}_4/\text{coke}$  composite as a heterogeneous Fenton-like catalyst. *Science of the Total Environment*, *574*, 1326–1334.
- Wang, S. B. (2008). A comparative study of Fenton and Fenton-like reaction kinetics in decolourisation of wastewater. *Dyes & Pigments*, *76*, 714–720.
- Wang, N. N., Chen, J. Q., Zhao, Q., & Xu, H. (2017a). Study on preparation conditions of coal fly ash catalyst and catalytic mechanism in a heterogeneous Fenton-like process. *RSC Advances*, *7*(83), 52524–52532.
- Wang, N. N., Zhao, Q., & Zhang, A. L. (2017b). Catalytic oxidation of organic pollutants in wastewater via a Fenton-like process under the catalysis of  $\text{HNO}_3$ -modified coal fly ash. *RSC Advances*, *7*(44), 27619–27628.
- Wu, Y., Luo, H. J., Wang, H., Zhang, L., Liu, P. P., & Feng, L. Q. (2014). Fast adsorption of nickel ions by porous graphene oxide/sawdust composite and reuse for phenol degradation from aqueous solutions. *Journal of Colloid & Interface Science*, *436*, 90–98.
- Xu, H. Y., Shi, T. N., Zhao, H., Jin, L. G., Wang, F. C., Wang, C. Y., & Qi, S. Y. (2016). Heterogeneous Fenton-like discoloration of methyl orange using  $\text{Fe}_3\text{O}_4/\text{MWCNTs}$  as catalyst: Process optimization by response surface methodology. *Frontiers of Materials Science*, *10*(1), 45–55.
- Yang, S. J., He, H. P., Wu, D. Q., Chen, D., Liang, X. L., Qin, Z. H., Fan, M. D., & Zhu, J. X. (2009). Decolorization of methylene blue by heterogeneous Fenton reaction using  $\text{Fe}_3\text{-xTi}_x\text{O}_4$  ( $0 \leq x \leq 0.78$ ) at neutral pH values. *Applied Catalysis B Environmental*, *89*, 527–535.
- Yu, L., Chen, J. D., Liang, Z., Xu, W. C., Chen, L. M., & Ye, D. Q. (2016). Degradation of phenol using  $\text{Fe}_3\text{O}_4$ -GO nanocomposite as a heterogeneous photo-Fenton catalyst. *Separation & Purification Technology*, *171*, 80–87.
- Zhang, S. X., Zhao, X. L., Niu, H. Y., Shi, Y. L., Cai, Y. Q., & Jiang, G. B. (2009). Superparamagnetic  $\text{Fe}_3\text{O}_4$  nanoparticles as catalysts for the catalytic oxidation of phenolic and aniline compounds. *Journal of Hazardous Materials*, *167*, 560–566.
- Zhao, S. F., Ma, H. J., Wang, M., Cao, C. Q., Xiong, J., Xu, Y. S., & Yao, S. D. (2010). Role of primary reaction initiated by 254 nm UV light in the degradation of p-nitrophenol attacked by hydroxyl radicals. *Photochemical & Photobiological Sciences: Official Journal of the European Photochemistry Association and the European Society for Photobiology*, *9*(5), 710–715.
- Zhu, S. M., Dong, B. Z., Yu, Y. H., Bu, L. J., Deng, J., & Zhou, S. Q. (2017). Heterogeneous catalysis of ozone using ordered mesoporous  $\text{Fe}_3\text{O}_4$  for degradation of atrazine. *Chemical Engineering Journal*, *328*, 527–535.
- Zubir, N. A., Yacou, C., Motuzas, J., Zhang, X., & Costa, J. C. D. D. (2014). Structural and functional investigation of graphene oxide- $\text{Fe}_3\text{O}_4$  nanocomposites for the heterogeneous Fenton-like reaction. *Scientific Reports*, *4*, 1–8.